coatings

MDPI

Article

The Device Using a Polydimethylsiloxane Membrane and the Phase Transition of Water

Yan Deng, ZiJian Chen, YinBo Zhu, HengAn Wu and Ping Gu *

CAS Key Laboratory of Mechanical Behavior and Design of Materials, CAS Center for Excellence in Complex System Mechanics, Department of Modern Mechanics, University of Science and Technology of China, Hefei 230027, China; dengyan@mail.ustc.edu.cn (Y.D.); czj0101@mail.ustc.edu.cn (Z.C.); zhuyinbo@ustc.edu.cn (Y.Z.); wuha@ustc.edu.cn (H.W.)
* Correspondence: guping@ustc.edu.cn

Abstract: The accumulation of ice on surfaces can cause harm in many industries. Our work describes an experiment and a simulation of the deicing effect based on a simple device combining a polydimethylsiloxane (PDMS) membrane and water phase transition. The device resulted in a minimum ice adhesion strength of 0.327 kPa, and the ice adhesion strength was still less than 5 kPa after 15 cycles, which meets the requirements of automatic deicing. It also held up after flushing with water and sand currents. In addition, our finite element simulation illustrates that the ice adhesion strength decreases greatly due to the change in initial stress distribution and the separation mode of ice. The fracture between the ice and membrane initiates from one side, and propagates gradually along the contour of ice while at the same time spreading rapidly towards the center. Compared with other icephobic methods, such as expensive and vulnerable micro/nano-surfaces or functional composite coatings, this low-cost and environment friendly device appears promising for large-scale deicing applications in various engineering fields.

Keywords: deicing; ice adhesion strength; separation mode; phase transition

Citation: Deng, Y.; Chen, Z.; Zhu, Y.; Wu, H.; Gu, P. The Device Using a Polydimethylsiloxane Membrane and the Phase Transition of Water. *Coatings* **2021**, *11*, 1102. https://doi.org/10.3390/coatings11091102

Academic Editor: George Kokkoris

Received: 31 July 2021
Accepted: 9 September 2021
Published: 13 September 2021

1. Introduction

Ice accumulation causes great economic losses and severe harm, especially in cold regions. Traditional deicing methods possess obvious defects, such as environmental pollution, massive energy consumption, damage to structural surfaces and threats to the safety of cleaners [1–7].

Inspired by the water repulsion of lotus leaves, superhydrophobic surfaces with micro/nano-structures are studied extensively for anti-icing/deicing [8–10]. Air cavitation between water droplets and a hydrophobic, rough surface delays ice nucleation and decreases the contact area between the ice and the surface, which lowers the ice's adhesion strength [10–12]. However, recent reports proved that the adhesion strength between ice and a hydrophobic, rough surface is greater than that of flat surface in high-humidity and low-temperature environment, because mechanical interlocking occurs when water enters into the micro/nano-structure gradually and freezes [13,14].

The ice's adhesion strength is evaluated by the fracture mechanics formula $\tau = \sqrt{\frac{E*G}{\pi\alpha\Lambda}}$, where E, G, α and Λ represent the apparent elastic modulus, surface energy, crack length and non-dimensional constant determined by the geometric configuration of the crack [15]. Lower ice adhesion strength can be obtained if the volume-adjusted elastic modulus and surface energy of the substrate are smaller. Through surface modifications with plasma, fluorination and lubricating fluid, surface energy will decrease. Inspired by Nepenthes, self-lubricating icephobic elastomer coatings are able to provide lubricating layers on solid surfaces, which can let ice slide off automatically [16–22]. Golovin et al. fabricated PDMS coatings with an oil layer to maintain the low adhesion strength of less than 10 kPa after 100 icing/deicing cycles [23]. He et al. designed PDMS coatings with sub-structures to

promote crack initiation at the ice–solid interface, and the minimal ice adhesion strength was 0.9 kPa [15,24–26]. However, the ice adhesion strength of a coating will increase significantly if the lubricant is removed from the surface by water [27].

Functional composite coatings also show great promise for icephobic applications. Li et al. obtained electrolyte hydrogel surfaces by infusing salted water into a hydrogel, and ice can be removed from the surface via self-weight within 10 s at −10 °C [28]. Liu et al. integrated a superhydrophobic copper mesh with intelligent organogel that can secrete an anti-freezing agent at subzero temperatures [29]. A coating using the photothermal effect of carbon black particles can melt ice on the surface in the sunlight. Wu et al. combined candle soot strengthened by a silica shell with grafted PDMS brushes to develop an anti-icing coating that ice could not form on until −50 °C [30]. Wu et al. prepared films combining hierarchically macro/micro-structured PDMS and reduced graphene oxide, and the minimal adhesion strength was 0.2 kPa [31]. However, the functional additives to these surfaces, such as carbon black particles, are easily taken away, and it is difficult to maintain good durability and stability for them.

The phase swelling force generated during water icing can be used to deice. Chen et al. designed a device combining a biaxially oriented polypropylene (BOPP) film and a 6061 aluminum alloy plate/PMMA plate to reduce the ice adhesion strength [32,33]. The adhesion strength was as low as 0 kPa when pits in the plates were filled with pure water, and the adhesion strength was 20–40 kPa when filled with an ethanol solution [32]. However, the deicing mechanism was not clearly explained.

In this work, we fabricated a simple and low-cost deicing device with a PMMA substrate and a PDMS membrane. The flexible PDMS, with low surface energy and a small elastic modulus, is an ideal candidate material for deicing [34]. The expansion force generated by water freezing in the holes of the PMMA surface performs active deicing. The ice adhesion strength of device's surface was measured by using a self-built test platform. The deicing ability of the device in harsh environments was explored via soaking, flushing and wearing it for different amounts of time. The deicing mechanism was also explored via simulation and fracture theory. Our work provides guidance for active deicing.

2. Materials and Methods

2.1. Preparation of the Deicing Device

A mixture of the PDMS prepolymer and the curing agent (184 Silicone Elastomer, Dow Corning, Midland, MI, USA) in the weight ratio of 10:1 was stirred thoroughly on a magnetic stirrer, and gas bubbles were removed by vacuuming. The process is shown in Figure 1. One milliliter of the mixture was dropped on a PMMA plate (Tmall, Hangzhou, China) and then rotated at 500 R/min for 1 s in the spin coater (Kejing instrument, Shenyang, China). Subsequently, it was cured at 60 °C for 12 h and the PDMS membrane was torn off carefully. Hole arrays with the depth of 4 mm were drilled on the PMMA plates, of 80 mm × 60 mm × 5 mm (L × W × H). Next, membranes and PMMA substrates were cleaned with an ethanol solution. The deionized water was injected into the holes with a syringe carefully, and a membrane was put on the surface of each PMMA substrate. The details of all the experimental groups are shown in Table 1. Groups A–C had only one hole; groups D and E had 3 × 3 hole arrays with homogeneous spacing of 8 mm; group F was a PMMA plate with a PDMS membrane, which was used as the control group.

Table 1. Details of groups A–F, and p represents the ratio of the area of holes to the area of the ice_t.

Group	A	B	C	D	E	F
Number of holes	1	1	1	3 × 3	3 × 3	0
Diameter/mm	30	28	25	4	4.5	0
p	0.694	0.605	0.482	0.111	0.141	0

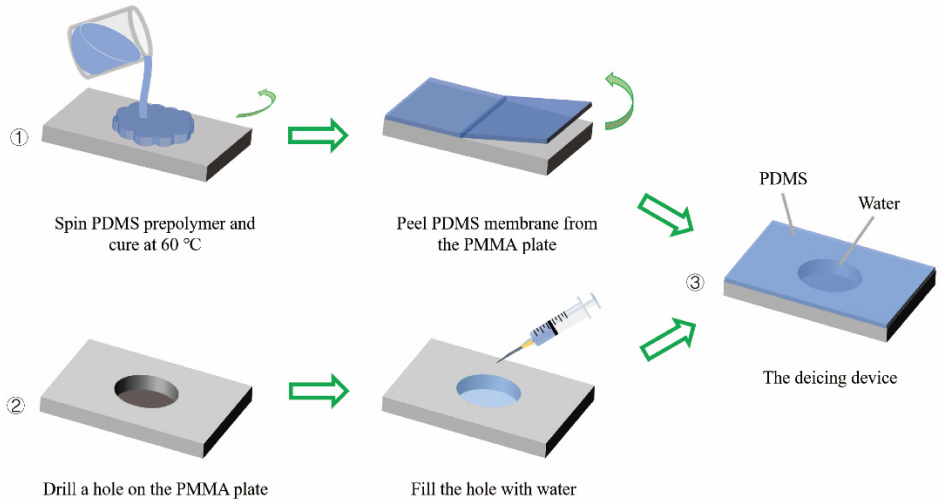

Figure 1. The fabrication process of the deicing device.

2.2. Characterization

The pull-off force needed for the ice was measured by the self-built testing platform, as shown in Figure 2a, which can provide a loading force between 0–50 N. The force resolution is 1 mN, and the sliding displacement resolution is 4 μm. The deicing device was fixed on the testing platform and a cylindrical PMMA tube (inner diameter of 36 mm, outer diameter of 40 mm and height of 20 mm) was placed on the device. Then 3 mL of deionized water was poured into the tube. In order to facilitate the description, we deonte the ice in the holes and tube as ice_h and ice_t, respectively. The platform was placed in a refrigerator (Xiamen Tawa Enterprise Co., Xiamen, China) at −20 °C. The thickness of the ice_h was about 5 mm. The pressure sensor was connected with the tube, and the stepping motor was activated, moving at a constant speed of 0.028 mm/s. The connecting point was as close to the ice–PDMS interface as possible. The force applied was recorded synchronously. The ice adhesion strength is defined as the maximum pulling force divided by the tube area. The ice shear strength of each group was averaged over three runs. The transmittance of the device was measured by the UV spectrophotometer (Shimadzu, Kyoto, Japan). The experiments shown in Figure 2b,c were used to study the flushing effect of water and sand currents. The vertical distance between the funnel and the sample was 50 cm, and the inner diameter of the funnel was 5.5 mm. The diameters of sea sand particles (Shanghai Chemical Reagent Co., Ltd., Shanghai, China) were 650–850 μm.

2.3. Finite Element Simulation

The ice delamination from the surface of the deicing device was analyzed by finite element simulation in ABAQUS. The influence of the PMMA substrate was ignored as the membrane was fixed on the substrate. Considering that the difference between stiffness of ice and PDMS is quite large, and no obvious deformation of ice_t was observed in the experiment, the ice on the PDMS surface was simplified as a rigid cylinder with a height of 1 mm and a diameter of 5 mm. The PDMS was set as neo-Hookean solid with Young's modulus E = 2.72 MPa and Poisson's ratio ν = 0.47 [35]. The thickness and diameter of the PDMS membrane were 0.5 mm and 15 mm respectively. Then, the membrane was meshed into about 300,000 C3D8RH elements and about 200,000 C3D6H elements in ABAQUS. The ice was considered to be in adhesive contact with the PDMS membrane. The vertical load acting on the bottom of PDMS membrane was applied to simulate the expansion force of water freezing.

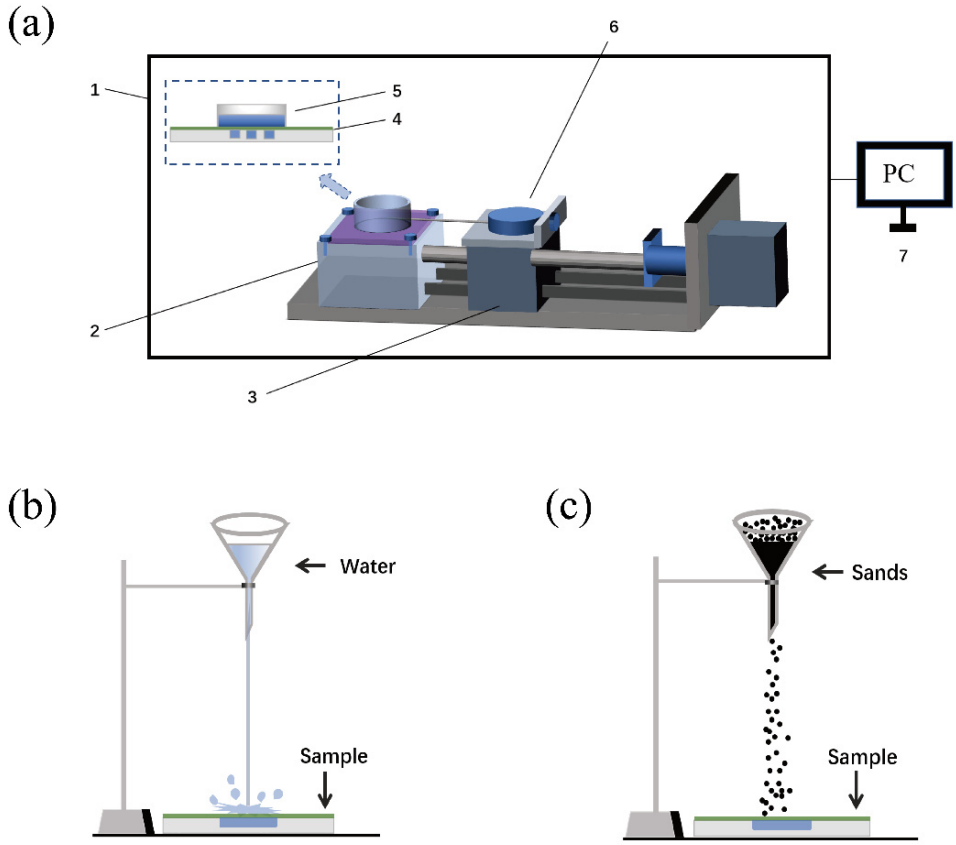

Figure 2. (**a**) Platform for the ice adhesion strength measurements: (1) refrigerator, (2) fixed platform, (3) stepper motor, (4) deicing device, (5) cylindrical tube, (6) force sensor, (7) computer; (**b**) the flushing of water; (**c**) the flushing of sand currents.

3. Results

3.1. Ice Adhesion Test

In order to explore the effect of cooling time, the ice adhesion strength values of group A were measured after being put in refrigerator under −20 °C for 2–18 h. As shown in Figure 3a, the ice adhesion strengths after cooling times of 2 and 3 h were much greater than those after 4–18 h. It was observed that the water in the tube had been frozen, but the water in the holes was not frozen completely, which led to insufficient expansion force acting on the bottom of the PDMS membrane. When the freezing time was longer than 3 h, the detaching force was almost constant. The expansion force generated by the water freezing in the hole acts on the bottom of the PDMS membrane, the bottom of the ice is unstuck from the PDMS surface and does not form new ice-membrane bonds over time again. The results also demonstrate sequential icing in the tube and hole due to different icing environments. The water in the tube was directly exposed to the atmosphere, which led to easier heat conduction, whereas the water in the hole was trapped by the PMMA plate and PDMS membrane with poor thermoconductivity. In addition, the water in the hole was more difficult to freeze due to greater pressure during the icing process.

Figure 3b shows the ice shear strength for groups A–F after 4 h of cooling at −20 °C. Group F was the flat PMMA plate covered with a PDMS membrane. The ice shear strength in group F was 118 kPa, whereas the ice shear strengths in groups A–E were less than 2 kPa. The minimum value was only 0.327 kPa—group A. This proves that the device has significant deicing power. The surface area ratio of the holes to ice_t is defined as p, as presented in Table 1. Comparing groups A, B and C, it can be concluded that the ice shear strength decreased as p increased. For the hole arrays, group E, with the largest value of p, also showed smaller ice shear strength to group D, as shown in Figure 3b. This could be explained by the larger diameter of the hole meaning more water freezing and

more expansion. Nevertheless, group E showed lower ice adhesion strength—even less than groups B and C, which means that the deicing effect of the device can be improved by changing the distribution of holes, and not merely relying on the increase of p. The appropriate hole array distribution and the right diameter for each hole may increase the deicing effect significantly.

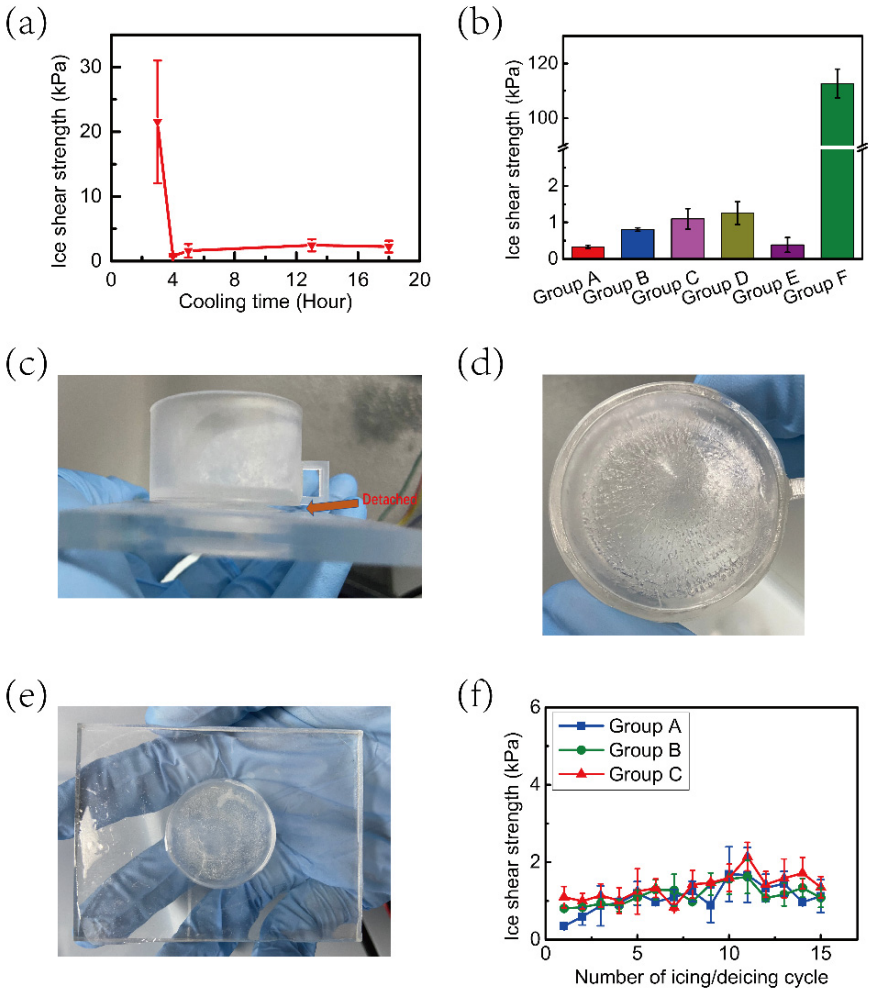

Figure 3. (**a**) The ice shear strength for group A after cooling times from 2 h to 18 h. (**b**) The ice shear strength of the group A–F. (**c**) The side view of icet. (**d**) The basal image of the icet. (**e**) The surface topography of the device after icet is detached. (**f**) The ice shear strength during 15 cycles.

The volume of frozen water in the hole expands, lifting up the ice in the cylindrical tube. The area around the bottom of the ice_t is separated from the PDMS membrane, as shown in Figure 3c. After the icet was pulled off from the membrane, the surface morphologies of the bottom of ice_t and the PDMS membrane could be seen. As shown in Figure 3d, the bottom of ice_t showed no significant deformations (pits, crushing, etc.) and some white spots were distributed within ice_t. As shown in Figure 3e, the membrane deformation was spherical, convex; and ice_h had a large amount of white broken ice slag, which was caused by the expansion impacting the bottom of the soft membrane and the subsequent stress concentration.

The durability of PDMS was verified in the experiments. The membrane was removed after the deicing testing, cleaned with alcohol and dried. The membrane was re-attached to the surface of the PMMA substrate and the adhesion strength of the ice was measured. As shown in Figure 3f, the ice adhesion strength remained below 5 kPa after 15 cycles, which proves that the device can be reused. This was due to the PDMS membrane itself forming stable adhesion on the PMMA substrate without the help of additional adhesives.

In addition, PDMS membrane, as a very flexible ultra-elastic material, can still remain intact after multiple loading/unloading cycles.

3.2. Mechanical Stability

When an engineering surface is exposed to the outdoor environment, the flushing of rainwater and wearing of sand will affect the membrane's adhesion to the substrate, and thus deicing performance. The water and sand current velocity were 1.503 m/s and 0.140 m/s, respectively. All adhesion strength values were less than 3 kPa, which proves that the device can resist certain harsh environments. The ice adhesion strength did not increase significantly within 0–30 min of scouring time, as shown in Figure 4a. As the sand flushing time increased, the ice adhesion strength gradually increased, as shown in Figure 4b. This is understandable because the water seeping into the tiny scratches left on the PDMS's surface caused by the sharp edges of the sand grains increased the valid icing area. However, there was no obvious damage on the surface of the membrane, and PDMS absorbed the energy carried by the grains through its own deformation.

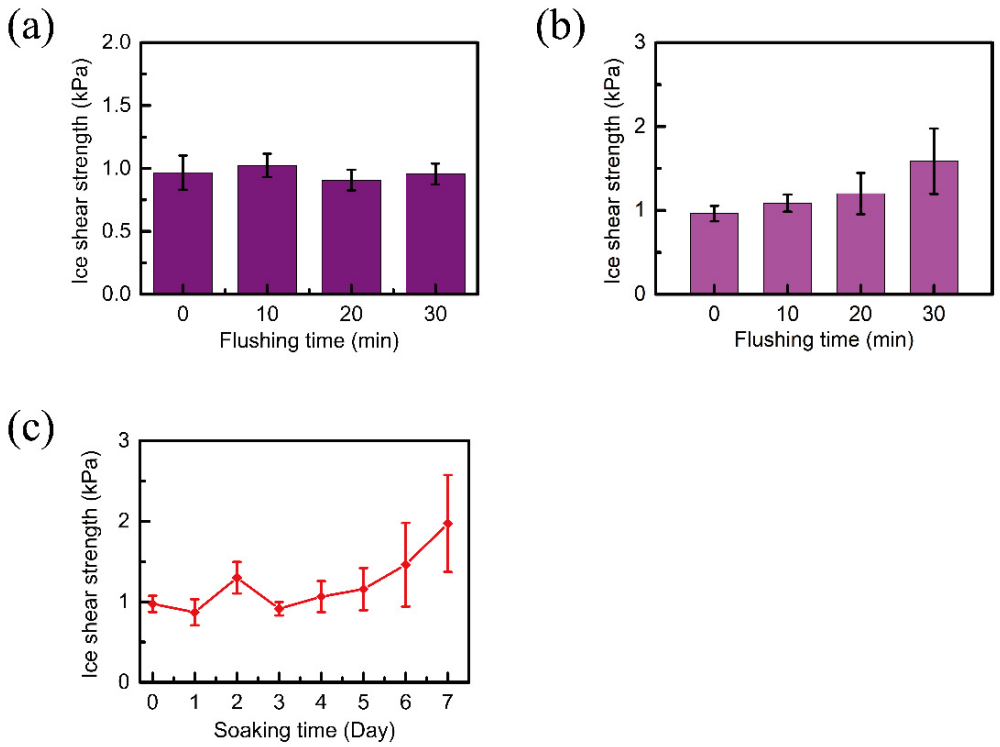

Figure 4. The ice shear strength after (**a**) flushing of water, (**b**) flushing of sand currents, (**c**) immersion in water for various durations.

The device was immersed in water for different amounts of time, and the ice adhesion strength was measured in −20 °C after 4 h of cooling. As shown in Figure 4c, ice adhesion strength increased as immersion time increased, but it was still less than 3 kPa, which proves the device can maintain excellent stability in a humid environment for a long time. The increase in shear strength may have been caused by the cleaner surface of the PDMS membrane and the water infiltration into the tiny pores of the membrane.

3.3. Transmittance Test

Due to high transparency of PDMS and PMMA, the device may be used for special surface deicing. For example, it could be used for surfaces with high-light transmittance requirements, such as integrated photovoltaic systems. The transmittance values of the PMMA plate; the PMMA plate with the PDMS membrane; and the PMMA plate–water–PDMS sample were measured at 400–1000 nm by a UV spectrophotometer. As shown in Figure 5a, the PMMA plate itself showed light transmittance greater than 90%, and

the PMMA plate with the PDMS membrane showed light transmittance of nearly 90%. This verified the high transparency of PDMS and PMMA. However, the visible light transmittance of the device dropped to between 60% and 70%. The bottom of the hole in our device was very rough due to the drilling process, which might have decreased transparency and increased the light reflection. On the other hand, it is possible that the beam suffered losses caused by reflections and refractions of the PDMS–water and water–PMMA interfaces. As shown in Figure 5b, two small bulbs connected in series with the solar panel were luminous when the solar panel covered by the deicing device was exposed under natural light.

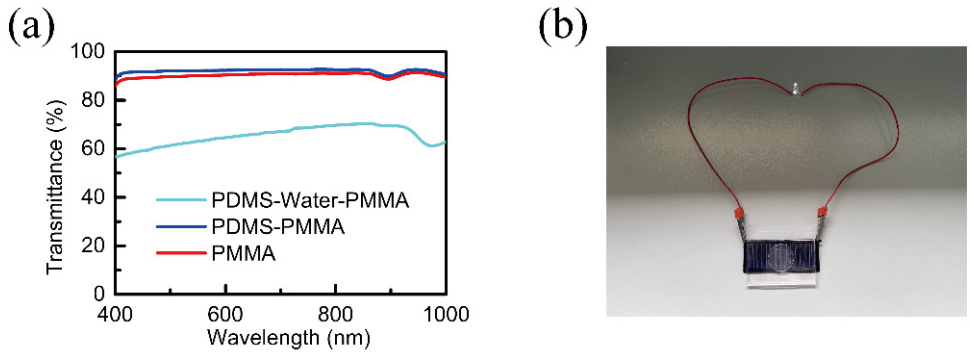

Figure 5. (**a**) The comparison of transmittance at 400–1000 nm. (**b**) The practical test of transmittance under natural light.

4. Discussion

A cylindrical rigid body with a diameter of 5 mm and an elastic substrate were used to define the ice_t and PDMS membrane, respectively, as shown in Figure 6a. The delamination of the ice from the membrane was studied with/without vertical load acting on the bottom of the membrane via FEM simulation, as schematically shown in Figure 7c. The expansion force caused by phase change of water in the hole was simulated with a vertical load applied to the bottom of the PDMS membrane. The vertical load was distributed in the circular area with a radius of 2 mm at the bottom of the membrane, with a maximum value of 0.072 MPa at the center of the membrane and a minimum value of 0 MPa at the edge. The reason for applying loading in this way is that the surface bulge is arc-shaped after the water in the pit freezes, which means the displacement at the edge of the pit is zero and the displacement at the center is the largest. The load varies with the time according to the simplified force–time curve in Chen's study [36]. The displacement-controlled loading was applied horizontally to the ice_t surface right above the ice–membrane interface. The pull-off force and delamination process were then systematically studied.

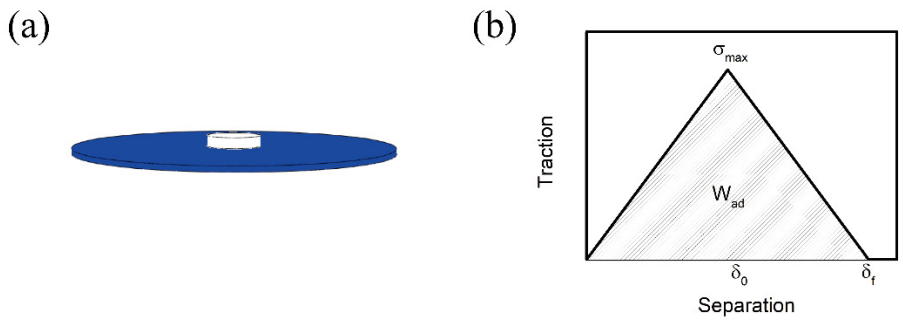

Figure 6. (**a**) The 3D model of finite element simulation. (**b**) Cohesive zone model.

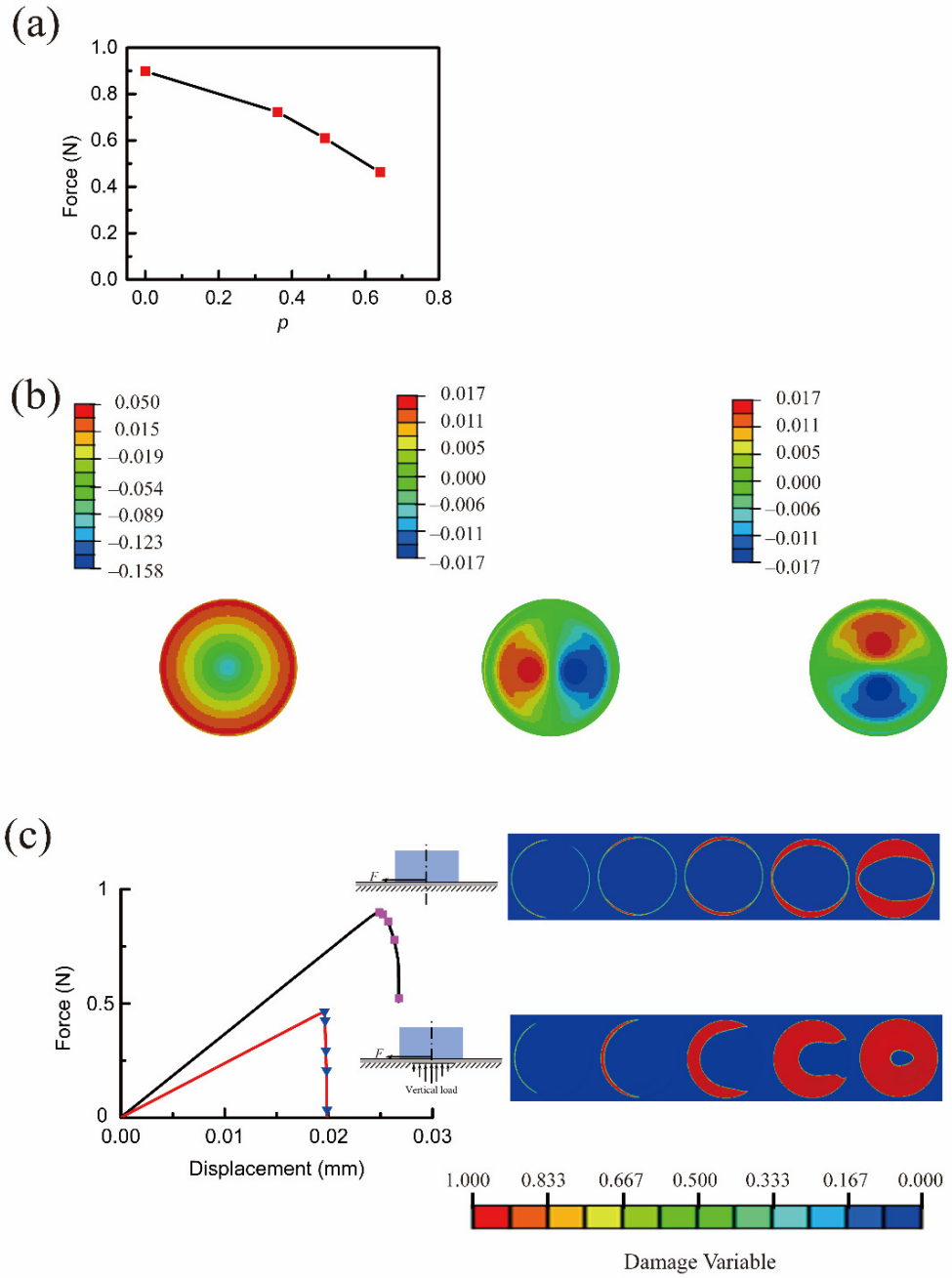

Figure 7. (**a**) Pull-off force varying with p (the ratio of the area of holes to the area of ice$_t$). (**b**) Normal and tangential stress distribution on the membrane's surface. (**c**) The process of ice separation from the surface is characterized by damage variable when p is equal to 0.64, and the red area represents separated. The red and black lines represent force–displacement curves during the separation process with/without the expansion load acting.

The cohesive zone model described by a bi-linear traction–separation law, as shown in Figure 6b, was used to define the adhesion between ice and membrane, which prescribes relative separation and mechanical traction between the two adhesive surfaces. Damage initiation will occur when the separation reaches δ_0 and the maximum separation δ_f will lead to complete failure of the interface. The adhesion energy W_{ad} which is equal to the area under the traction–separation curve represents the required energy for separation in a unit area. When the energy release rate of the interface crack G reaches the value of W_{ad}, interface separation initiates to occur. Since the performance of cohesive zone model is not very sensitive to the actual shape of the traction-separation curve, δ_0 was set as 0.005 mm

and δ_f was equal to 0.01 mm, based on our previous experience. What truly matters is the area under the traction–separation curve. Since it is not easy to measure the adhesion energy between ice and PDMS membrane, the W_{ad} was assumed to be 0.0005 N/mm according to the fracture energy of polyurethane and ice [37].

In Abaqus, damage initiation is required to satisfy a quadratic stress criterion based on Equation (1). The process of interface fracture can be quantitatively observed by calculating the damage variable D, which is obtained from Equation (2). The value of D ranges from 0 to 1, and a value of 1 indicates complete separation [38]:

$$\left(\frac{\sigma_n}{\sigma_{\max}}\right)^2 + \left(\frac{\sigma_s}{\sigma_{\max}}\right)^2 + \left(\frac{\sigma_t}{\sigma_{\max}}\right)^2 = 1 \quad (1)$$

$$D = \frac{\delta_f(\delta_m - \delta_0)}{\delta_m\left(\delta_f - \delta_0\right)} \quad (2)$$

where σ_n, σ_s, and σ_t represent the normal and two shear traction forces. The loading process is controlled by displacement.

Figure 7a shows the relationship between the required force and p during the simulation of the separation process. When p was equal to 0.64 the maximum pull-off force was reduced to 46.21% compared to that without an expansion load. As the area the expansion force was acting on increased, the required pull-off force of removing ice from the surface decreased—a tendency consistent with our experimental results.

From the perspective of deformation, when the expansion load acts on the bottom of the membrane, the soft PDMS membrane deforms and become thinner because PDMS is nearly incompressible. However, the deformation of the membrane surface in the adhesion area is hindered due to the stable adhesion between the ice layer and the PDMS membrane. In addition, the membrane around the interface between ice and PMDS is also subject to the boundary constraints of the hole edge. Therefore, the surrounding region of the holes will generate relatively large normal stress and shear stress under the action of expansion load. As shown in Figure 7b, the normal stress reached 0.05 MPa, and the shear stress reached 0.017 MPa. When ice is separated from the membrane surface under the pull-off force, the energy release rate G_{edge} at the contact area edge can be calculated with normal stress σ_{zz} and shear stress σ_{xz} according to Equation (3), where K_{I} and K_{II} are stress intensity factors of Mode I and Mode II [39]. When G_{edge} is equal to W_{ad}, the bonding edges initiate separation. Due to the higher stress distribution at the edge caused by the expansion load, the initial crack intensity factors K and G_{edge} are increased, which further promotes the detaching process of ice from surface and also leads to a change in the detaching process.

$$\begin{gathered} \sigma_{zz} = \frac{K_{\mathrm{I}}}{\sqrt{2\pi x}}, \sigma_{xz} = \frac{K_{\mathrm{II}}}{\sqrt{2\pi x}}\ x \to 0 \\ G_{edge} = \frac{(1-v^2)}{2E}\left[K_{\mathrm{I}}^2 + K_{\mathrm{II}}^2\right] \end{gathered} \quad (3)$$

As shown in Figure 7c, when a horizontal pulling force along the positive x-axis is applied to ice$_t$ in the absence of an expansion load, the crack first only initiates along the lateral edge of the ice$_t$, and then propagates to the surroundings and center. However, when the expansion load is applied, the delamination starts at the front of the left half edge, and spreads to the center and the right half, and eventually the ice debonds.

Although the trend of the simulation results is the same as that of the experiments, there are some differences. It was observed in the experiments that part of the surrounding area of the ice was separated before the pulling force was applied, but not in the simulation. A discrepancy between the actual load and assumed one should account for the difference. The impact load was produced by water's phase change, whereas a static load was applied in the simulation. In addition, the distribution of the force generated by icing at the bottom of the film is complex, as the water in the hole is limited by the membrane and PMMA substrate, so the average value adopted in the simulation affected the results. The separated

area can be regarded as the initial crack, so it can be inferred that the force required for separation will be greatly reduced, because a change of crack size from 0.01 mm to 1 mm means that the shear strength will be reduced by 10 times [11]. In conclusion, it is proven that our device combining soft materials and expanding loads is beneficial for removing ice from surfaces.

5. Conclusions

A simple and reusable active deicing device was prepared by filling the holes of PMMA plates with deionized water and attaching a PDMS membrane to the PMMA's surface. The device shows good deicing ability: the ice adhesion strength can be lower than 5 kPa, which meets the requirements of self-weight deicing. Due to the difference in phase transition time, after the membrane forms stable adhesion with the ice on the surface, the water in the holes freezes and produces an expansion force that acts on the bottom of the membrane. The considerable stiffness difference between the solid ice and soft material results in uncoordinated deformation and a large stress distribution, which change the debonding mode of the ice–membrane interface and promote the separation of ice from the surface. The device still maintains low adhesion after flushing with water and sand currents. It also maintains high transparency and optical transmittance. In summary, in addition to excellent deicing capabilities, our device based on a soft membrane and the phase change of water has the advantages of environmental protection, simple fabrication, low cost and reusability. It shows great potential for deicing engineering surfaces.

Author Contributions: Conceptualization, Y.D.; methodology, Y.D.; software, Z.C.; validation, Y.D. and P.G.; formal analysis, Y.D.; investigation, Y.D. and Y.Z.; resources, H.W.; data curation, Y.D.; writing—original draft preparation, Y.D.; writing—review and editing, P.G. and Y.Z.; visualization, Y.D. and Z.C.; supervision, P.G.; project administration, P.G. and H.W.; funding acquisition, P.G. and H.W. All authors have read and agreed to the published version of the manuscript.

Funding: This work was supported by the Major Program of the National Science Foundation of China (number 11890683), the Strategic Priority Research Program of the Chinese Academy of Sciences (XDB22040402) and the National Natural Science Foundation of China (11872063).

Institutional Review Board Statement: Not applicable.

Informed Consent Statement: Not applicable.

Data Availability Statement: Not applicable.

Acknowledgments: The authors are grateful to the CAS Key Laboratory of Mechanical Behavior and Design of Materials (LMBD) and the USTC Center for Micro- and Nanoscale Research and Fabrication.

Conflicts of Interest: The authors declare no conflict of interest.

References

1. Andersson, P.-O.; Jelle, B.P.; Zhang, Z. Passive Snow Repulsion: A State-of-the-art Review Illuminating Research Gaps and Possibilities. *Energy Procedia* **2017**, *132*, 423–428. [CrossRef]
2. Caliskan, F.; Hajiyev, C. A review of in-flight detection and identification of aircraft icing and reconfigurable control. *Prog. Aerosp. Sci.* **2013**, *60*, 12–34. [CrossRef]
3. Chen, H.; Wu, Y.; Xia, H.; Jing, B.; Zhang, Q. Review of ice-pavement adhesion study and development of hydrophobic surface in pavement deicing. *J. Traffic Transp. Eng.* **2018**, *5*, 224–238. [CrossRef]
4. Dalili, N.; Edrisy, A.; Carriveau, R. A review of surface engineering issues critical to wind turbine performance. *Renew. Sustain. Energy Rev.* **2009**, *13*, 428–438. [CrossRef]
5. Hu, L.; Zhu, X.; Hu, C.; Chen, J.; Du, Z. Wind turbines ice distribution and load response under icing conditions. *Renew. Energy* **2017**, *113*, 608–619. [CrossRef]
6. Jha, P.; Brillembourg, D.; Schmitz, S. Wind Turbines Under Atmospheric Icing Conditions—Ice Accretion Modeling, Aerodynamics, and Control Strategies for Mitigating Performance Degradation. In Proceedings of the 50th AIAA Aerospace Sciences Meeting including the New Horizons Forum and Aerospace Exposition, Nashville, TN, USA, 9–12 January 2012.
7. Yirtici, O.; Ozgen, S.; Tuncer, I.H. Predictions of ice formations on wind turbine blades and power production losses due to icing. *Wind Energy* **2019**, *22*, 945–958. [CrossRef]

8. Das, S.; Kumar, S.; Samal, S.K.; Mohanty, S.; Nayak, S.K. A Review on Superhydrophobic Polymer Nanocoatings: Recent Development and Applications. *Ind. Eng. Chem. Res.* **2018**, *57*, 2727–2745. [CrossRef]
9. Hejazi, V.; Sobolev, K.; Nosonovsky, M. From superhydrophobicity to icephobicity: Forces and interaction analysis. *Sci. Rep.* **2013**, *3*, 2194. [CrossRef]
10. Yu, T.; Lu, S.; Xu, W.; Boukherroub, R. Preparation of superhydrophobic/superoleophilic copper coated titanium mesh with excellent ice-phobic and water-oil separation performance. *Appl. Surf. Sci.* **2019**, *476*, 353–362. [CrossRef]
11. Nosonovsky, M.; Hejazi, V. Why Superhydrophobic Surfaces Are Not Always Icephobic. *ACS Nano* **2012**, *6*, 8488–8491. [CrossRef] [PubMed]
12. Wang, G.; Liu, S.; Wei, S.; Liu, Y.; Lian, J.; Jiang, Q. Robust superhydrophobic surface on Al substrate with durability, corrosion resistance and ice-phobicity. *Sci. Rep.* **2016**, *6*, 20933. [CrossRef] [PubMed]
13. Chen, J.; Liu, J.; He, M.; Li, K.; Cui, D.; Zhang, Q.; Zeng, X.; Zhang, Y.; Wang, J.; Song, Y. Superhydrophobic surfaces cannot reduce ice adhesion. *Appl. Phys. Lett.* **2012**, *101*, 111603. [CrossRef]
14. Kreder, M.J.; Alvarenga, J.; Kim, P.; Aizenberg, J. Design of anti-icing surfaces: Smooth, textured or slippery? *Nat. Rev. Mater.* **2016**, *1*, 1–15. [CrossRef]
15. He, Z.; Zhuo, Y.; Wang, F.; He, J.; Zhang, Z. Understanding the role of hollow sub-surface structures in reducing ice adhesion strength. *Soft Matter* **2019**, *15*, 2905–2910. [CrossRef]
16. Cui, W.; Pakkanen, T.A. Icephobic performance of one-step silicone-oil-infused slippery coatings: Effects of surface energy, oil and nanoparticle contents. *J. Colloid Interface Sci.* **2020**, *558*, 251–258. [CrossRef]
17. He, Z.; Wu, C.; Hua, M.; Wu, S.; Wu, D.; Zhu, X.; Wang, J.; He, X. Bioinspired Multifunctional Anti-icing Hydrogel. *Matter* **2020**, *2*, 723–734. [CrossRef]
18. Wang, F.; Ding, W.; He, J.; Zhang, Z. Phase transition enabled durable anti-icing surfaces and its DIY design. *Chem. Eng. J.* **2019**, *360*, 243–249. [CrossRef]
19. Yeong, Y.H.; Milionis, A.; Loth, E.; Sokhey, J. Self-lubricating icephobic elastomer coating (SLIC) for ultralow ice adhesion with enhanced durability. *Cold Reg. Sci. Technol.* **2018**, *148*, 29–37. [CrossRef]
20. Yeong, Y.H.; Wang, C.; Wynne, K.J.; Gupta, M.C. Oil-Infused Superhydrophobic Silicone Material for Low Ice Adhesion with Long-Term Infusion Stability. *ACS Appl. Mater. Interfaces* **2016**, *8*, 32050–32059. [CrossRef]
21. Zhao, L.; He, L.; Liang, J.; Chen, Y.; Jia, M.; Huang, J. Facile preparation of a slippery oil-infused polymer surface for robust icephobicity. *Prog. Org. Coat.* **2020**, *148*, 105849. [CrossRef]
22. Wong, T.-S.; Kang, S.H.; Tang, S.K.Y.; Smythe, E.J.; Hatton, B.D.; Grinthal, A.; Aizenberg, J. Bioinspired self-repairing slippery surfaces with pressure-stable omniphobicity. *Nature* **2011**, *477*, 443–447. [CrossRef]
23. Golovin, K.; Kobaku, S.P.R.; Lee, D.H.; DiLoreto, E.T.; Mabry, J.M.; Tuteja, A. Designing durable icephobic surfaces. *Sci. Adv.* **2016**, *2*, e1501496. [CrossRef] [PubMed]
24. He, Z.; Xiao, S.; Gao, H.; He, J.; Zhang, Z. Multiscale crack initiator promoted super-low ice adhesion surfaces. *Soft Matter* **2017**, *13*, 6562–6568. [CrossRef] [PubMed]
25. He, Z.; Zhuo, Y.; He, J.; Zhang, Z. Design and preparation of sandwich-like polydimethylsiloxane (PDMS) sponges with super-low ice adhesion. *Soft Matter* **2018**, *14*, 4846–4851. [CrossRef] [PubMed]
26. He, Z.; Zhuo, Y.; Wang, F.; He, J.; Zhang, Z. Design and preparation of icephobic PDMS-based coatings by introducing an aqueous lubricating layer and macro-crack initiators at the ice-substrate interface. *Prog. Org. Coat.* **2020**, *147*, 105737. [CrossRef]
27. Heydarian, S.; Jafari, R.; Momen, G. Recent progress in the anti-icing performance of slippery liquid-infused surfaces. *Prog. Org. Coat.* **2021**, *151*, 106096. [CrossRef]
28. Li, T.; Ibanez-Ibanez, P.F.; Hakonsen, V.; Wu, J.; Xu, K.; Zhuo, Y.; Luo, S.; He, J.; Zhang, Z. Self-Deicing Electrolyte Hydrogel Surfaces with Pa-level Ice Adhesion and Durable Antifreezing/Antifrost Performance. *ACS Appl. Mater. Interfaces* **2020**, *12*, 35572–35578. [CrossRef]
29. Liu, F.; Wang, Z.; Pan, Q. Intelligent Icephobic Surface toward Self-Deicing Capability. *ACS Sustain. Chem. Eng.* **2019**, *8*, 792–799. [CrossRef]
30. Wu, S.; Du, Y.; Alsaid, Y.; Wu, D.; Hua, M.; Yan, Y.; Yao, B.; Ma, Y.; Zhu, X.; He, X. Superhydrophobic photothermal icephobic surfaces based on candle soot. *Proc. Natl. Acad. Sci. USA* **2020**, *117*, 11240–11246. [CrossRef] [PubMed]
31. Wu, C.; Geng, H.; Tan, S.; Lv, J.; Wang, H.; He, Z.; Wang, J. Highly efficient solar anti-icing/deicing via a hierarchical structured surface. *Mater. Horiz.* **2020**, *7*, 2097–2104. [CrossRef]
32. Chen, T.; Cong, Q.; Li, Y.; Jin, J.; Choy, K.-L. Utilizing swelling force to decrease the ice adhesion strength. *Cold Reg. Sci. Technol.* **2018**, *146*, 122–126. [CrossRef]
33. Chen, T.; Jin, J.; Qi, Y.; Tian, W.; Cong, Q.; Choy, K.-L. Disturbing stability of interface by adopting phase-change temperature gradient to reduce ice adhesion strength. *Cold Reg. Sci. Technol.* **2019**, *158*, 69–75. [CrossRef]
34. Liu, J.; Wang, J.; Mazzola, L.; Memon, H.; Barman, T.; Turnbull, B.; Mingione, G.; Choi, K.-S.; Hou, X. Development and evaluation of poly(dimethylsiloxane) based composite coatings for icephobic applications. *Surf. Coat. Technol.* **2018**, *349*, 980–985. [CrossRef]
35. Muller, A.; Wapler, M.C.; Wallrabe, U. A quick and accurate method to determine the Poisson's ratio and the coefficient of thermal expansion of PDMS. *Soft Matter* **2019**, *15*, 779–784. [CrossRef] [PubMed]

36. Chen, T. Research on Active Anti/De-Icing Method Based on Disturbing the Adhesion Stability of Ice-Solid Interface (In Chinese). Ph.D. Thesis, Jilin University, Changchun, China, 2019.
37. Andrews, E.H.; Majid, H.A.; Lockington, N.A. Adhesion of ice to a flexible substrate. *J. Mater. Sci.* **1984**, *19*, 73–81. [CrossRef]
38. Sun, X.; Yu, L.; Rentschler, M.; Wu, H.; Long, R. Delamination of a rigid punch from an elastic substrate under normal and shear forces. *J. Mech. Phys. Solids* **2019**, *122*, 141–160. [CrossRef]
39. Lin, Y.Y.; Hui, C.-Y.; Conway, H.D. A Detailed Elastic Analysis of the Flat Punch (Tack) Test for Pressure-Sensitive Adhesives. *J. Polym. Sci. Part B Polym. Phys.* **2000**, *38*, 2769–2784. [CrossRef]